Evolving nuclear many-body forces with the similarity renormalization group

E. D. Jurgenson[*]

Lawrence Livermore National Laboratory, P. O. Box 808, L-414, Livermore, California 94551, USA

P. Navrátil[†]

Lawrence Livermore National Laboratory, P. O. Box 808, L-414, Livermore, California 94551, USA and TRIUMF,
4004 Wesbrook Mall, Vancouver, British Columbia, V6T 2A3 Canada

R. J. Furnstahl[‡]

Department of Physics, The Ohio State University, Columbus, Ohio 43210, USA

In recent years, the Similarity Renormalization Group has provided a powerful and versatile means to soften interactions for *ab initio* nuclear calculations. The substantial contribution of both induced and initial three-body forces to the nuclear interaction has required the consistent evolution of free-space Hamiltonians in the three-particle space. We present the most recent progress on this work, extending the calculational capability to the *p*-shell nuclei and showing that the hierarchy of induced many-body forces is consistent with previous estimates. Calculations over a range of the flow parameter for ^{6}Li, including fully evolved $NN + 3N$ interactions, show moderate contributions due to induced four-body forces and display the same improved convergence properties as in lighter nuclei. A systematic analysis provides further evidence that the hierarchy of many-body forces is preserved.

I. INTRODUCTION

A major goal of nuclear structure theory is to make quantitative calculations of low-energy nuclear observables starting from microscopic internucleon forces. Renormalization group (RG) methods can be used to soften the short-range repulsion and tensor components of available initial interactions so convergence of nuclear structure calculations is greatly accelerated [1,2]. A major complication is that these transformations change the short-range many-body forces. In fact, any softening transformation will induce many-body interactions in the course of renormalizing the matrix elements in a lower sector. To account for these changes, we must include consistently evolved three-body (and possibly higher) forces in structure calculations.

A previous letter [3] presented the first such evolution of three-body forces in free space by using the Similarity Renormalization Group (SRG) [4–9]. The SRG offers an approach to evolving many-body forces that is technically simpler than other unitary RG formulations. Irrespective of the chosen initial Hamiltonian, the evolution produces a variational Hamiltonian and enables smooth extrapolation of results, in contrast to Lee-Suzuki [10] type transformations which produce results that are model-space dependent (in both N_{max} and A) [11]. While the SRG induces many-body forces as a product of renormalization, these terms come in a hierarchy of decreasing strength if a hierarchy is initially present. Particularly useful in an analysis of such a hierarchy are chiral effective field theories (χEFTs), which provide a

systematic construction of many-body forces as the initial input to our evolution calculations [12]. Our results expand on prior evidence that the SRG explicitly preserves the initial EFT many-body hierarchy as it improves convergence properties of evolved Hamiltonians.

Section II reviews some background material on how the SRG is applied in these calculations. In Sec. III we explore the convergence properties of the renormalized Hamiltonians, including new $A = 6$ calculations. In Sec. IV we present the calculations as a function of the evolution parameter and explore the effect of SRG flow on other initial interactions. Section V dives deeper into the analysis of how the SRG acts to evolve the input interaction, expanding on the analysis done for one-dimensional models [13]. We make a brief advertisement of operator evolution and conclude with comments on the future use of this approach.

II. BACKGROUND

As implemented in Refs. [7,8] for nuclear physics, the SRG is a series of unitary transformations, U_λ, of the free-space Hamiltonian,

$$H_\lambda = U_\lambda H_{\lambda=\infty} U_\lambda^\dagger , \tag{1}$$

labeled by a momentum parameter λ that runs from ∞ toward zero, which keeps track of the sequence of Hamiltonians ($s = 1/\lambda^4$ is also used elsewhere [7,8]). These transformations are implemented as a flow equation in λ (in units where $\hbar^2 = M = 1$),

$$\frac{dH_\lambda}{d\lambda} = -\frac{4}{\lambda^5}[[T, H_\lambda], H_\lambda], \tag{2}$$

whose form guarantees that the H_λ's are unitarily equivalent [6,7]. Once the Hamiltonian has been evolved we also have the

———————
[*]jurgenson2@llnl.gov
[†]navratil@triumf.ca
[‡]furnstahl.1@osu.edu

option to build the unitary transformation operator directly as a sum over outer products of the evolved and unevolved wave functions:

$$U_\lambda = \sum_\alpha |\psi_\alpha(\lambda)\rangle\langle\psi_\alpha(0)|, \quad (3)$$

where α is an index over the states in the chosen configuration space. This feature is useful in applications to external operators [14]. Note that U_λ can also be evolved directly and the choice of method is open to efficiency and convenience for a particular use.

The appearance of the nucleon kinetic energy T in Eq. (2) leads to high- and low-momentum parts of H_λ being decoupled, which means softer and more convergent potentials [15]. This is evident in a partial-wave momentum basis, where matrix elements $\langle k|H_\lambda|k'\rangle$ connecting states with kinetic energies differing by more than λ^2 are suppressed by $e^{-(k^2-k'^2)^2/\lambda^4}$ factors and therefore the states decouple as λ decreases. However, decoupling also results from replacing T in Eq. (2) with other operators [6,7,16,17]. The optimal range for λ is not yet established and also depends on the system. Previous experience with SRG and other low-momentum potentials suggested that running to about $\lambda = 2.0$ fm^{-1} is a good compromise between improved convergence from decoupling and the growth of induced many-body interactions [15]. Current results show that this limit might be extended as far as $\lambda = 1.0$ fm^{-1}, at least for lighter nuclei.

One formal way to see how the two-, three-, and higher-body potentials evolve is to decompose H_λ in second-quantized form [6]. We can write a general A-body Hamiltonian as:

$$H_\lambda = \sum_{ij} T_{ij} a_i^\dagger a_j + \frac{1}{2!^2} \sum_{ijkl} V_{ijkl,\lambda}^{(2)} a_i^\dagger a_j^\dagger a_l a_k$$
$$+ \frac{1}{3!^2} \sum_{ijklmn} V_{ijklmn,\lambda}^{(3)} a_i^\dagger a_j^\dagger a_k^\dagger a_n a_m a_l + \cdots, \quad (4)$$

where $a_i^\dagger$ and a_i are creation and destruction operators with respect to the vacuum in some single-particle-momentum basis. The quantities T_{ij}, $V_{ijkl}^{(2)}$, and $V_{ijklmn}^{(3)}$ denote matrix elements of their respective operators. Equation (4) *defines* T_{ij}, $V_{ijkl,\lambda}^{(2)}$, $V_{ijklmn,\lambda}^{(3)}$, ..., as the one-body, two-body, three-body, ..., matrix elements at each λ. By evaluating the commutators in Eq. (2) using H_λ from Eq. (4), and normal ordering the resulting terms of creation/annihilation operators, we find that higher-body potentials are generated with each step in λ, even if initially there are only two-body potentials. We note that in this article we are not actually evolving in a single-particle basis as indicated in Eq. (4), but nothing *a priori* prevents it as a choice of basis. In particular, the center-of-mass (c.m.) solutions will factor out in the properly truncated harmonic oscillator single-particle basis. Furthermore, the SRG will not mix different center-of-mass solutions since $T_{c.m.}$ commutes with the Hamiltonian.

Here we are normal ordering with respect to the vacuum, as opposed to the in-medium SRG which normal orders with respect to a nonvacuum reference state. With in-medium normal ordering, SRG evolution generates an A-dependent

rearrangement of the higher-body contributions to the evolved interaction; the density-dependent zero-, one-, and two-body normal-ordered interactions are found to absorb the dominant free-space many-body interactions [18]. For free-space normal ordering, matrix elements in a given sector are determined completely by evolution in that sector. In addition, each A-body sector contains as a subset the $(A-1)$-body sector evolutions. Thus, when applied in an A-body subspace, the SRG will "induce" A-body forces, with $\langle T \rangle$ fixed, $\langle V_\lambda^{(2)}\rangle$ determined completely in the $A = 2$ subspace with no dependence on $\langle V_\lambda^{(3)}\rangle$, $\langle V_\lambda^{(3)}\rangle$ determined in $A = 3$ given $\langle V_\lambda^{(2)}\rangle$ and $\langle V_{\lambda=0}^{(3)}\rangle$, and so on.

Because only the Hamiltonian enters the SRG evolution equations, there are no difficulties from having to solve T matrices (of the Lippmann-Schwinger equation) in all channels for different A-body systems [1]. However, in a momentum basis the presence of spectator nucleons requires solving separate equations for each set of $\langle V^{(n)}\rangle$ matrix elements. In Ref. [19], a diagrammatic approach was introduced to handle this decomposition. But while it is natural to solve Eq. (2) in momentum representation, it is an operator equation allowing us to use any convenient basis. Here we evolve in a *discrete* basis of Jacobi-coordinate harmonic oscillator wave functions, where spectators are handled without a decomposition and induced many-body interaction matrix elements can be directly identified. Having chosen a basis, we obtain coupled first-order differential equations for the matrix elements of the flowing Hamiltonian H_λ, where the right side of Eq. (2) is evaluated using simple matrix multiplications.

The procedures used here build directly on Ref. [13], which presents a one-dimensional implementation of our approach along with a general analysis of the evolving many-body hierarchy. We start by evolving H_λ in the $A = 2$ subsystem, which completely fixes the two-body matrix elements $\langle V_\lambda^{(2)}\rangle$. Next, by evolving H_λ in the $A = 3$ subsystem we determine the combined two-plus-three-body matrix elements. We can isolate the three-body matrix elements by subtracting the evolved $\langle V_\lambda^{(2)}\rangle$ elements in the $A = 3$ basis [13]. Having obtained the separate *NN* and *NNN* matrix elements, *we can apply them unchanged to any nucleus*. We are also free to include any initial three-nucleon force in the initial Hamiltonian without changing the procedure. If applied to $A \geqslant 4$, four-body (and higher) forces will not be included and so the transformations will be only approximately unitary. The questions to be addressed are whether the decreasing hierarchy of many-body forces is maintained and whether the induced four-body contribution is unnaturally large. We summarize in Table I the different calculations to be made here for ^{3}H, ^{4}He,

TABLE I. Definitions of the various calculations.

NN-only:	No initial *NNN* interaction and do not keep *NNN*-induced interaction.
NN + *NNN*-induced:	No initial NNN interaction but keep the SRG-induced *NNN* interaction.
NN + *NNN*:	Include an initial *NNN* interaction *and* keep the SRG-induced *NNN* interaction.

and ^{6}Li to confront these questions. These calculations will also be made when other nuclei are considered.

Hamiltonians obtained via free-space SRG evolution are independent of the basis choice. Up to truncations induced by conversion to a particular basis, a Hamiltonian evolved to a given λ reproduces the results of a Hamiltonian evolved to the same λ in a different basis. Two types of truncations, in model-space size and A, are relevant to controlling the quality and consistency of SRG evolved interactions. Our calculations are performed in the Jacobi coordinate harmonic oscillator (HO) basis of the no-core shell model (NCSM) [20]. This is a translationally invariant, antisymmetric basis for each A-body sector, in which a complete set of states in the model space defines the maximum excitation of $N_{max}\hbar\Omega$ above the minimum energy configuration, where Ω is the harmonic oscillator parameter. Hamiltonians are derived and evolved in this basis and then switched to a Slater determinant basis. The Jacobi coordinates used to build this basis have a convenient normalization that treats all A-body clusters on an equal footing. Operators in an A-body space, like the A-body Hamiltonian, can be embedded in an $(A + n)$-body space in a straightforward manner. Due to the antisymmetric nature of the basis, they need only be multiplied by a combinatoric factor:

$$\binom{A + n}{A} = \frac{(A + n)!}{A!(n)!} . \tag{5}$$

For example, a three-body system has $\binom{3}{2} = 3$ pairs, a four-body system has $\binom{4}{2} = 6$ pairs, and $\binom{4}{3} = 4$ triplets, and so on. This embedding factor was a direct predictor of behavior in one dimension [13], but in the realistic case, many physical constraints may complicate the end results, including, but not limited to, Pauli blocking, angular momentum selection rules, and cancellations intrinsic to the initial Hamiltonian.

A major drawback of the HO basis is its single intrinsic scale, $\hbar\Omega$, which is problematic for systems with multiple scales. However, it is a widely used basis in part because it facilitates the separation of spurious center-of-mass solutions and vital to the translationally invariant physics of nuclear structure calculations. To understand the cutoffs inherent in the finite oscillator basis we can consider that the local maxima in the harmonic oscillator function are essentially Gaussians modulated by polynomial terms up to N_{max}. These maxima, in the momentum and coordinate space representations, will be correlated with the high- and low-momentum cutoffs respectively. These cutoffs have the large N_{max} behavior [21]

$$\Lambda_{UV} \sim \sqrt{mN_{max}\hbar\Omega} \quad \text{and} \quad \Lambda_{IR} \sim \sqrt{\frac{m\hbar\Omega}{N_{max}}}. \tag{6}$$

When $\hbar\Omega$ grows large, individual oscillations are large and lose resolution on the small details in the momentum basis potential that correspond to large r structures. However, high N_{max} polynomials have many small oscillations at low momenta compensating for the large $\hbar\Omega$ value. Thus, Λ_{IR} is lowered and Λ_{UV} is raised by increasing N_{max} as expected when the basis is extended toward completeness. Note that only the value of N_{max}, not $\hbar\Omega$, affects the number of matrix elements in the basis, so the computational cost is the same for

TABLE II. Definitions of the truncations used on initial Hamiltonians.

N_{max}:	The size of the final A-body space
N_{A3max}:	The size of the basis for initial three-body matrix elements
N_{A2max}:	The size of the basis for initial two-body matrix elements

each $\hbar\Omega$. Changing $\hbar\Omega$ effects the balance between Λ_{IR} and Λ_{UV} completeness.

Note that the behavior attributed to Λ_{IR} does not manifest as an explicit cutoff in the momentum representation but rather a distortion of matrix elements at low momentum. Specifically, the effective cutoff operator in momentum representation displays bands of ringing artifacts along the off-diagonal direction that ultimately behave as a cutoff; both smaller $\hbar\Omega$ and larger N_{max} bases alleviate this effect, as is apparent from Eq. (6).

Because of computational constraints we were forced to apply separate truncations, N_{A2max} and N_{A3max}, to the $A = 2$ and $A = 3$ sectors of the initial Hamiltonian (see Table II). In previous work [3] with ^{3}H and ^{4}He and an initial χEFT interaction, we found that $N_{A2max} = N_{A3max} = 32$ was sufficient because these nuclei are less sensitive to the asymptotic behavior of the oscillator wave functions. However, for ^{6}Li or ^{4}He using a harder potential (such as Argonne V_{18}), larger space was required for the initial NN Hamiltonian. When needed we used $N_{A2max} = 300$, which is more than enough to accommodate any potential at any relevant $\hbar\Omega$. In some calculations we were restricted to $N_{A2max} = 196$, but these cases are also converged to the keV level. The $A = 3$ basis size grows much more quickly so the evolution of Hamiltonians above $N_{A3max} = 40$ are very intense computations. In our final results there is a slight effective truncation of the induced three-body forces, but this is only a truncation of the initial interaction that is then evolved. Additionally, the NNN interaction is a perturbative correction to the NN so this truncation has a small impact on our results. These truncation issues are addressed throughout the article when discussing the convergence properties of our results.

The present calculations make use of both the Jacobi oscillator basis described above and a Slater determinant oscillator basis often referred to as the m scheme. The size of the Jacobi basis scales well with N_{max} but poorly with A due to the effort involved in antisymmetrization. A Slater determinant basis trades ease of antisymmetrization for very large (dimensions into the billions) but sparse matrices, solvable with the Lanczos algorithm. Given the convergence advantages provided by the SRG, we obtain the initial Hamiltonians in the Jacobi basis, evolve them in $A = 2$ and 3, and transform them into a Slater determinant basis for use in existing configuration interaction (CI) codes.

Our calculations are limited by the size of the input three-body interaction file: The present code is not able to distribute the matrix elements among nodes and therefore must hold the entire A-body Hamiltonian on each node. For our calculations of ^{6}Li at $N_{max} = 8$, the three-body file is 13 Gb of matrix elements in addition to two-body matrix elements already stored. This is the largest calculation possible on most

available nodes with 16 or 32 Gb of memory; at $N_{max} = 10$ the three-body file is 33 Gb. However, the m-scheme code MFDn of Vary *et al.* [22] is capable of distributing the input matrix elements among several nodes and efforts are underway to perform these calculations in larger spaces. Furthermore, the size of these input files can be dramatically reduced in the future by implementing a compression scheme based on angular-momentum couplings and calculations could be extended with the importance truncation method [23,24]. Future calculations of ^{8}Be, ^{10}B, and ^{12}C are planned. Recent results of ^{12}C and ^{16}O using importance truncation provide a benchmark for future efforts [25].

For the lower λ's in the lighter nuclei, our predictions for ground-state energies are fully converged. However, in other cases we need to extrapolate the energies to $N_{max} = \infty$. Here we use the same extrapolation procedure applied in Ref. [2]. The model used for ground-state energies is

$$E_{\alpha i} = E_{\infty} + A_{\alpha}\, e^{-b_{\alpha} N_i}, \qquad (7)$$

where α labels the $\hbar\Omega$ values, i the N_{max} values for each α, and A_{α} and b_{α} are constants. The goal of a fit to the following calculations is to determine the common parameter E_{∞}, which is the estimate for the ground-state energy extrapolated to $N_{max} = \infty$.

This can be cast as a one-dimensional constrained minimization problem with the function

$$g(E_{\infty}) = \sum_{\alpha, i} [\log(E_{\alpha i} - E_{\infty}) - a_{\alpha} - b_{\alpha} N_i]^2 / \sigma_{\alpha i}^2, \qquad (8)$$

where the $\{a_{\alpha}\}$ and $\{b_{\alpha}\}$ are determined directly within the function g by invoking a constrained linear least-squares minimization routine. The constraint is the bound $E_{\infty} \leqslant \min(\{E_{\alpha i}\})$, where $E_{\infty} < 0$ and "min" means "most negative." We can also allow for weights depending on N_{max} and/or $\hbar\Omega$. In the present investigation, we apply Eq. (8) with only the $\hbar\Omega$ value that yields the lowest energy in the largest space, weighting different N_{max} by the slope of the energy vs. N_{max} and using the spread of results from neighboring $\hbar\Omega$ values to determine a conservative confidence interval for the extrapolation. Alternative approaches to extrapolation in the NCSM are described in Ref. [26].

We have considered a variety of interactions as initial inputs to the SRG evolution, including chiral EFT, Argonne V_{18} [27], and CD-Bonn [28]. The initial ($\lambda = \infty$) chiral NN potential is the 500-MeV N^{3}LO interaction from Ref. [29]. With the chiral potential we also have available an initial NNN potential at N^{2}LO [30] in the local form of Ref. [31], with constants $c_D = -0.2$ and $c_E = -0.205$ fit to the average of triton and ^{3}He binding energies and to triton β decay as described in Ref. [32]. NCSM calculations with these initial chiral interactions and the parameter set in Table I of Ref. [32] yield energies of $-8.473(4)$ MeV for ^{3}H and $-28.50(2)$ MeV for ^{4}He compared with -8.482 MeV and -28.296 MeV from experiment, respectively. There is a 20-keV uncertainty in the calculation of ^{4}He from incomplete convergence but a 200-keV discrepancy with experiment. The latter is consistent with the omission of three- and four-body chiral interactions at N^{3}LO [33]. These provide the scale for assessing whether induced four-body contributions are important compared to

other uncertainties. The best result for ^{4}He using the AV18 potential is $-24.23(1)$ MeV [34] and using CD-Bonn we compare to $-26.1(1)$ MeV. Here there are larger discrepancies with the experimental values due to the omission of consistent initial three-body interactions, but these calculations are still useful to assess the effects of induced NNN.

For ^{6}Li calculations we use only the chiral interactions at N^{3}LO [29] for NN and at N^{2}LO for NNN in the form described above. The best existing binding energy with the N^{3}LO interaction, using a Lee-Suzuki–based renormalization up to $N_{max} = 14$, is 28.5 ± 0.5 MeV. With NNN included the converged value is 32.5 ± 0.5 MeV [35]. The truncations analogous to N_{A2max} and N_{A3max} for these calculations were $N_{A2max} = 400$ and $N_{A3max} = 40$, equivalent to the initial Hamiltonian inputs for the present work. Results are generally not dependent on the particular values of the LECs in a range of $c_D \sim -2$ to $+2$ (with c_D and c_E constrained by the fit to ^{3}H [32]) but some observables may be particularly sensitive as discussed in Ref. [36].

III. CONVERGENCE

In Fig. 1, we show the triton ground-state energy as a function of the oscillator basis size, N_{max}. The convergence of the bare interaction is compared with the SRG evolved to $\lambda = 2.0$ and 1.5 fm^{-1}. The oscillator parameter $\hbar\Omega$ in each case was chosen to optimize the convergence of each Hamiltonian. We also compare to a Lee-Suzuki (LS) calculation (green squares), which has been used in the NCSM to greatly improve convergence [36,37]. All of these effective interactions result from unitary transformations. The LS is done within the model space of a target nucleus, in contrast to the free-space transformation of the SRG, which yields nucleus-independent matrix elements. Consequently, the LS results are nonvariational independent calculations at each N_{max} while the SRG-evolved Hamiltonians can be
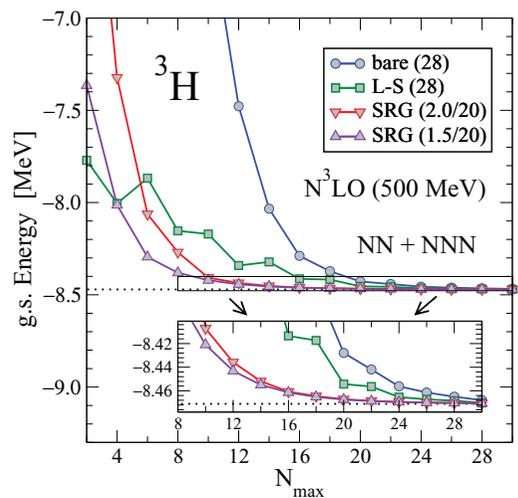

FIG. 1. (Color online) Ground-state energy of ^{3}H as a function of the basis size N_{max} for an N^{3}LO NN interaction [29] with an initial NNN interaction [12,32]. Unevolved ("bare") and Lee-Suzuki (L-S) results with $\hbar\Omega = 28$ MeV are compared with SRG evolved to $\lambda = 2.0$ fm^{-1} and 1.5 fm^{-1} with $\hbar\Omega = 20$ MeV.
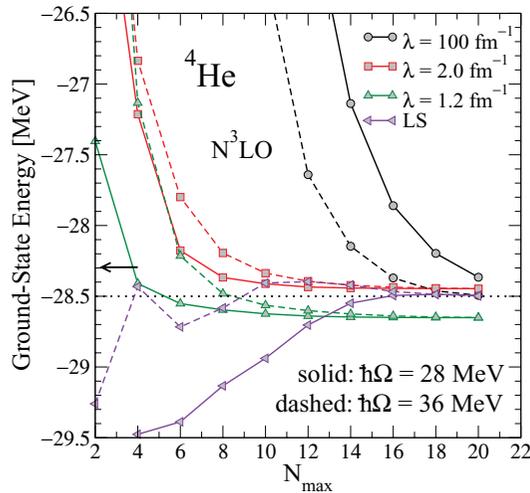
FIG. 2. (Color online) Ground-state energy of ^{4}He as a function of the basis size N_{max} for an N^{3}LO NN interaction [29] with an initial NNN interaction [12,32]. Unevolved (λ) results are compared with Lee-Suzuki (L-S) and SRG evolved to $\lambda = 2.0$ and 1.2 fm^{-1} at $\hbar\Omega = 28$ and 36 MeV. The black arrow indicates the experimental value.

simply truncated to produce the curves shown. A dramatic improvement in convergence rate compared to the initial interaction is seen even though the χEFT initial interaction is relatively soft. The SRG acts to decouple high-momentum degrees of freedom so the UV part converges faster with respect to N_{max}. Thus, once evolved, a much smaller N_{max} basis is adequate for a particular accuracy.

Figure 2 illustrates for ^{4}He the same rapid convergence with N_{max} of an SRG-evolved interaction. However, in this case the asymptotic value of the energy differs slightly because of the omitted induced four-body contribution. The difference can be as large as 100 keV for $\lambda = 1.0$ but no larger than 50 keV for the substantially evolved $\lambda = 2.0$ fm^{-1}. The SRG-evolved asymptotic values for different $\hbar\Omega$ (solid vs. dotted

curves) differ by only 10 keV, so the gap between the converged bare/L-S result and the SRG result is dominated by the induced $NNNN$ rather than incomplete convergence. Convergence is even faster for lower λ values, ensuring a useful range for the analysis of few-body systems. However, because of the strong density dependence of four-nucleon forces, it will be important to monitor the size of the induced four-body contributions for heavier nuclei and nuclear matter. In Sec. V we present a tool for analyzing the growth of induced many-body forces.

Also evident in Fig. 2 is the evolving dependence on $\hbar\Omega$. Calculations are variational in $\hbar\Omega$ with the optimal value indicating balance between Λ_{UV} and Λ_{IR}. For the initial Hamiltonian, the limit of $N_{max} = 20$ is small and the larger $\hbar\Omega$ is necessary to provide a sufficient Λ_{UV}. The larger IR cutoff due to higher $\hbar\Omega$ is less of a problem than the smaller UV cutoff due to the low N_{max}. However, if the initial Hamiltonian is evolved in the $N_{max} = 32$ space, then more UV information is shifted down into the $N_{max} = 20$ space. Now the high IR cutoff is more significant and a lower $\hbar\Omega$ is more optimal. In the figure, one can see that the $\hbar\Omega = 28$ calculation (solid curves) has significantly better convergence properties for lower λ, especially at the small N_{max} ($\leqslant 8$) that is crucial for larger A.

Evolving Hamiltonians such as Argonne V_{18} and CD-Bonn also results in much improved convergence properties, as seen in Figs. 3(a) and 3(b). Here a large initial $A = 2$ cutoff, N_{A2max}, is crucial due to the strong high-momentum components in the AV18 potential. However, at $N_{A2max} = 196$ the NN-only results are converged with respect to variation in N_{A2max} to within 1 keV. For CD-Bonn we found that $N_{A3max} = 40$ and $N_{max} = 20$ was sufficient to converge results to within 30 keV. Calculations for the Argonne potential require a bit more effort, obtaining convergence with respect to N_{A3max} to within 130 keV. The optimal frequency for both of these interactions evolved to $\lambda = 2.0$ was found to be $\hbar\Omega = 44$ MeV. Larger values for N_{A3max} are possible for these potentials, but the current level of convergence is sufficient to observe the qualitative behavior of the SRG in Sec. IV.
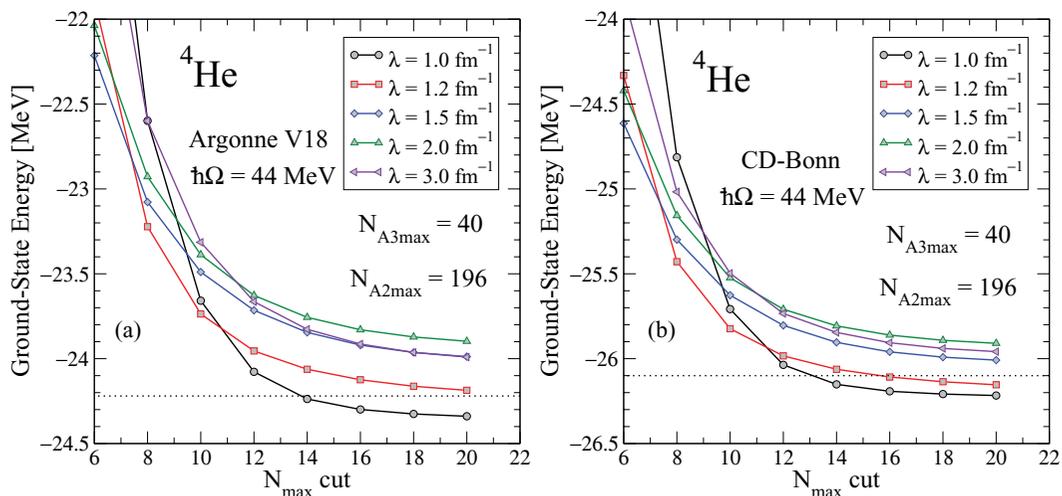

FIG. 3. (Color online) Ground-state energy of ^{4}He for select λ as a function of the basis size N_{max} for the (a) AV18 [27] and (b) CD-Bonn [28] interactions. Results are shown for $\hbar\Omega = 44$ MeV with $N_{A3max} = 40$. Dotted lines indicate current best results for these potentials [34].

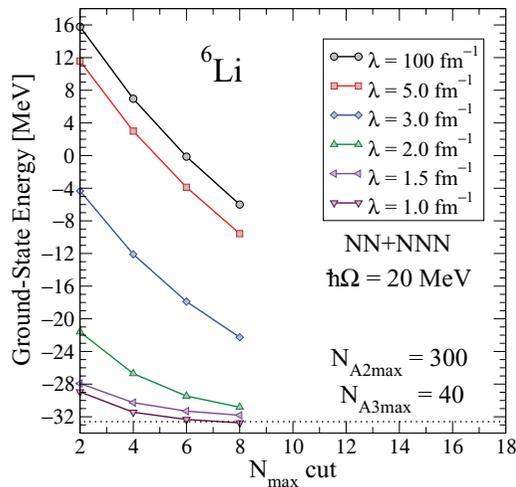FIG. 4. (Color online) Ground-state energy of ^{6}Li as a function of the basis size N_{max} for an initial N^{3}LO *NN* interaction [29] and an initial N^{2}LO *NNN* interaction [12,32] evolved to various λ. Note the large scale and complete lack of convergence for unsoftened Hamiltonians ($\lambda = 100$ fm^{-1}). The dotted line is the best Lee-Suzuki result.

A multitude of chiral EFT interactions are available for use in initial Hamiltonians. We have used here the one version (500 MeV N^{3}LO from Ref. [29]) for which the accompanying three-nucleon terms have been rigorously fit to data. An important task in the future will be to apply SRG techniques to many more available interactions to compare and contrast them. Some of these can be significantly harder than that chosen here, so running to low λ would be especially important though computationally expensive.

Figure 4 shows just how important a softening transformation is to achieve convergence in light nuclei. Here we plot ^{6}Li binding energies up to $N_{\text{max}} = 8$ for several λ's from 100 to 1.0 fm^{-1}. A meaningful extrapolation is simply not possible, even with the relatively soft chiral potential, without some form of softening renormalization like the SRG or Lee-Suzuki type transformations. A key advantage of the SRG program is

the ability to perform systematic extrapolations to spaces that are computationally inaccessible.

Compare this to the case of ^{4}He where the initial chiral EFT Hamiltonian is sufficiently soft to produce a nearly converged result at $N_{\text{max}} = 20$. For $A = 6$ we are restricted to smaller N_{max} because the basis scales with N_{max} much faster than at $A = 4$. In addition the radius of ^{6}Li is larger and requires a lower IR cutoff. Thus more oscillator basis states of the initial interaction are required to accurately describe this nucleus. In other words, even if we could perform the $N_{\text{max}} = 20$ calculation of ^{6}Li, it would still not converge as well as ^{4}He does at that level. With the SRG the information of the larger basis can be moved into a smaller space in a smooth controlled way.

In Fig. 5 we show the convergence patterns of the ground state of ^{6}Li on a more detailed scale. Here the three different calculations of Table I are shown side-by-side for clarity, with several λ values. The initial Hamiltonian was defined by the truncations $N_{\text{A2max}} = 300$ and $N_{\text{A3max}} = 40$ and the truncation errors from (or convergence with respect to) these limits are 1 and 80 keV respectively. The ^{6}Li calculation was performed up to $N_{\text{max}} = 8$ for the three-body matrix element versions, and $N_{\text{max}} = 10$ for *NN*-only (possible with only two-body matrix elements). Further calculations with three-body matrix elements will require a distributed memory approach like MFDn of Vary *et al.* [22] and the other techniques mentioned above; such codes will be used for future calculations of larger *p*-shell nuclei. The straight dotted line shows the converged Lee-Suzuki results for *NN*-only and *NN* + *NNN* calculations.

While we can see the improvement in convergence by the data points alone, we can only measure the effect of induced many-body forces by considering the extrapolated converged value for each λ. We provide a sample of the extrapolations we will use to assess the converged values for ^{6}Li, in the form of the dotted lines extending from each curve. The spread of these lines at large N_{max} is the chief indicator of remaining scale dependence in the results. In Fig. 5(a), which is *NN*-only, one can clearly see the large spread due to omitted induced three-body matrix elements. This spread is decreased in the other plots by including three-body matrix
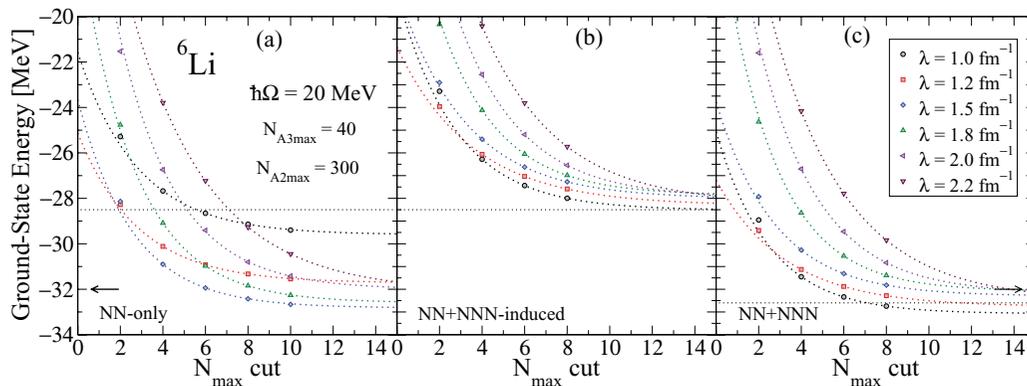

FIG. 5. (Color online) Ground-state energy of ^{6}Li as a function of the basis size N_{max} for an initial N^{3}LO *NN* interaction [29] and an initial N^{2}LO *NNN* interaction [12,32] evolved to various λ. Here the initial *NN* potential was included up to $N_{\text{A2max}} = 300$ and the *NNN* up to $N_{\text{A3max}} = 40$. Results are compared with the best Lee-Suzuki shown by the thin black dotted line (see text). The dotted lines extending from the curves are examples of the extrapolations made throughout.
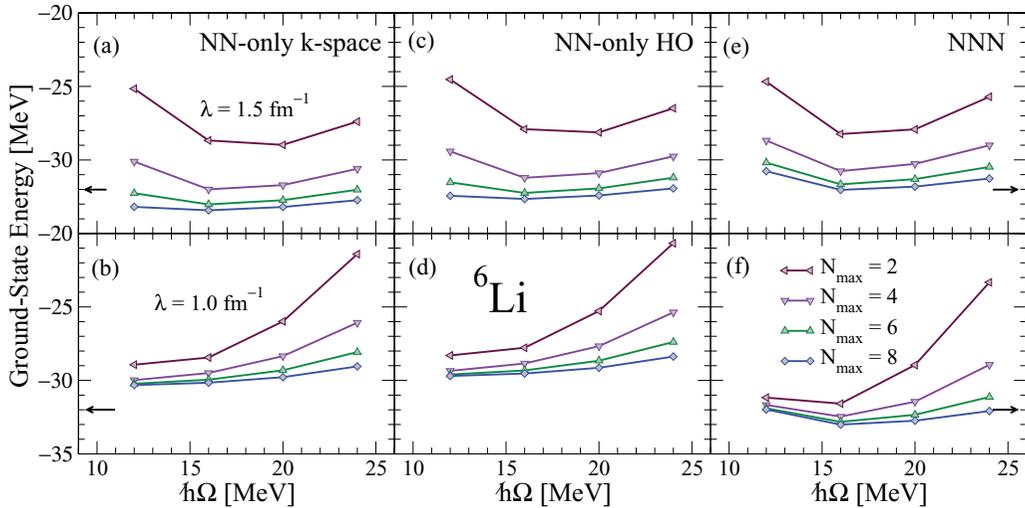
FIG. 6. (Color online) Ground-state energy of ^{6}Li as a function of the oscillator frequency, $\hbar\Omega$. Again we use a N^{3}LO *NN* [29] up to $N_{A2max} = 300$ and N^{2}LO *NNN* [12,32] up to $N_{A3max} = 40$. Panels (a)–(d) are *NN*-only while (e) and (f) include both induced and initial *NNN*. The black arrows indicate the experimental value. Note for comparison, the left is shifted relative to the center due to the difference in initial interactions.

elements, first, in Fig. 5(b) by including those induced by the renormalization and in Fig. 5(c) by including the initial *NNN* strength in the evolution. In both *NNN*-inclusive plots the curves have a smooth qualitative progression from higher to lower λ, indicating less interplay between attractive and repulsive components of the interaction, as discussed in Sec. V.

The size of induced four- to six-body forces in this calculation is estimated by measuring the spread of the lines in the center and right plots or, alternatively, by considering the slope of the binding energy as a function of λ. However, the spread is actually smaller than it appears here because only the $\lambda = 1.5$ and 1.8 curves are satisfactorily converged at this $\hbar\Omega$. The curves for other λ's are optimal at different values of $\hbar\Omega$ and their converged values are not accurately represented in this simple example. However, the full extrapolation procedure does indeed take this $\hbar\Omega$ dependence into account and this figure serves as a visual reminder of the process.

Finally, we mention the sensitivity of the extrapolations to the range in N_{max} used to fit the exponential function. Results at $N_{max} = 10$ with *NN*-only allow an assessment of the extrapolation procedure. We find that including the $N_{max} = 2$ points bias the extrapolation high, so the best estimates use $N_{max} = 4$–8 when *NNN* matrix elements are included.

Figure 6 shows the convergence of the ^{6}Li ground state as a function of $\hbar\Omega$ for selected λ's. The separate panels compare, for two different λ's (top and bottom), the current results with a previous study [2] of *NN*-only calculations where the evolutions were performed in momentum space. The momentum-space evolutions used only the neutron-proton part of the interaction, V_{np}, as an average for the complete *NN* interaction and added the Coulomb contribution separately afterward, causing a systematic overbinding of about 1 MeV. We have used the whole N^{3}LO [29] interaction and included the Coulomb in our evolutions but have checked that we recover the previous *NN*-only results with V_{np}. The left panel shows the momentum-space evolved calculations. The center

panel shows a reproduction of those results with a systematic shift due to the revised handling of the initial interaction. The right panel shows the full *NN* + *NNN* calculation. All three panels show good correspondence in $\hbar\Omega$ dependence between the previous and current calculations, indicating that the *NN*-only calculations are good predictors of the minima for the larger 3N-inclusive version.

As discussed above, a lower $\hbar\Omega$ results in a lower cutoff, Λ_{UV} [see Eq. (6)] and requires a larger basis (larger N_{max}) to achieve the same convergence. This can be seen in the *NN* + *NNN* panel by observing the trend in N_{max} for each $\hbar\Omega$. The values that each of the $\hbar\Omega$ spaces are converging toward differ, indicating that the initial Hamiltonian has been truncated by different incomplete bases and will not obtain the same result; the lowest N_{max} curve is not yet flat. This is especially evident at the smallest $\hbar\Omega$ which has the worst truncation. Improving this convergence requires increasing the three-body basis size, N_{A3max}. Here, at $N_{A3max} = 40$, the dimension of a single $A = 3$ channel (with quantum numbers $J^\pi T$) can be 7–8000 states, requiring 60–70 nodes for 12 h with a hybridized MPI-OpenMP evolution code. This is currently the most significant computational bottleneck in our SRG program.

In Fig. 7, we show the spectrum for ^{6}Li in absolute level energies on the left and excited state spacings on the right. We chose $\lambda = 1.8$ fm^{-1} due to sufficient convergence as indicated by our extrapolation procedure. This example happens to closely match the excitation spectrum of available LS based results, though the variation in λ is not large. We also include a spectrum with the excitation energies shifted to the converged ground-state energy.

The upper pair of plots shows the convergence with respect to the final N_{max} of the ^{6}Li calculation. In Fig. 7(a) we can see a consistent convergence pattern from $2\hbar\Omega$ down to $8\hbar\Omega$, but the results are clearly not converged at $8\hbar\Omega$. In Fig. 7(b), the excitation energies indicate that the higher
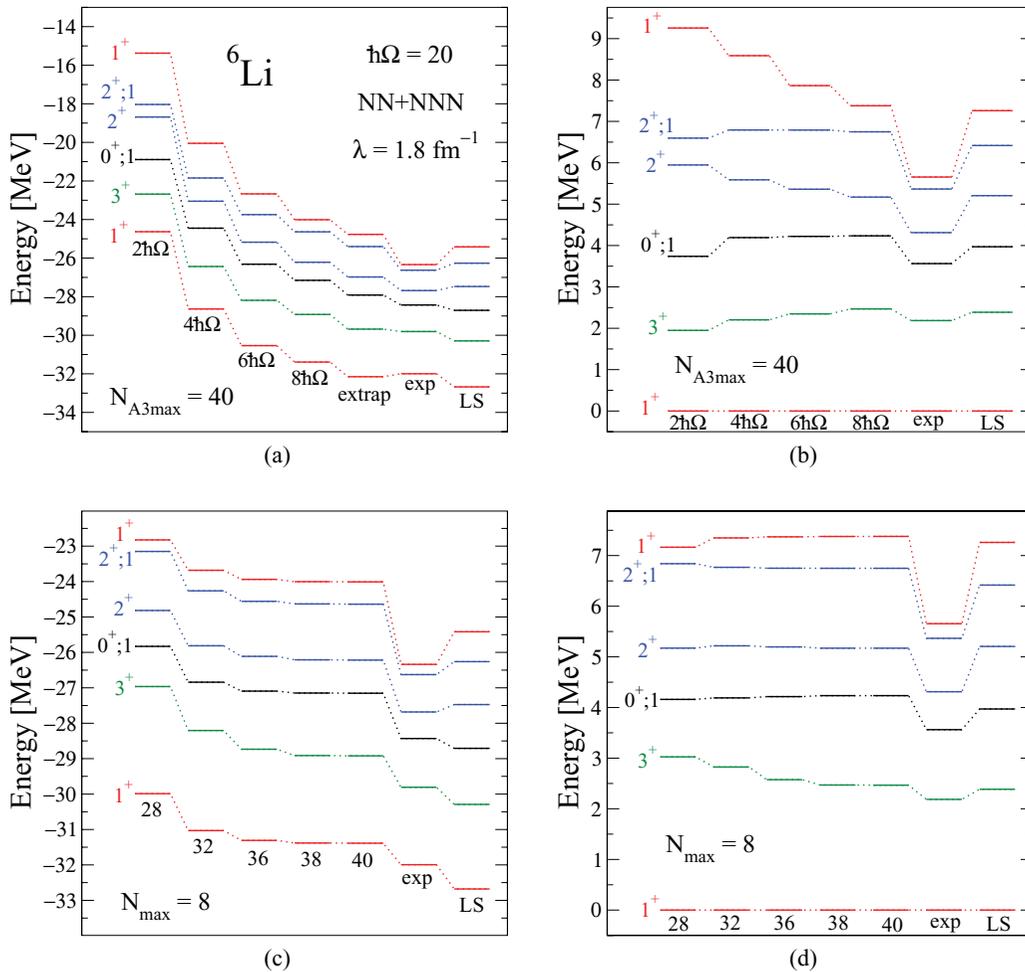
FIG. 7. (Color online) Spectrum of ^{6}Li as a function of N_{A3max}. Convergence in N_{max} is shown in (a) and (b) and convergence in N_{A3max} is shown in (c) and (d). Absolute energies are shown in (a) and (c) while excitation energies are used in (b) and (d). All four panels are for $\lambda = 1.8$ fm^{-1} with $NN + NNN$ at $\hbar\Omega = 20$ MeV and $N_{A2max} = 300$.

J states are converging more slowly due to stronger dependence on the higher $A = 3$ partial waves. This was tested by using various levels of truncation in the initial Hamiltonian for channels with higher values of J so, for example, if $J > 1$, then $N_{max} < N_{A3max}$ for that channel. We can also see here that the excitation energies compare well to the existing LS calculations.

The lower panels show the dependence on the initial truncation of the $A = 3$ sector, N_{A3max}. In Fig. 7(c) we see that the Hamiltonian is well converged when $N_{A3max} = 40$. In Fig. 7(d) the excitation energy of the 3^+ state drops significantly with increasing N_{A3max}. In these calculations, not only is N_{A3max} larger, but also individual channels are truncated less severely to provide more of the Hamiltonian for these higher-J states. Specifically, at $N_{A3max} = 36$ each step up in J corresponded to a reduction in N_{max} of 4. But, for the $N_{A3max} = 40$ calculations this was changed to 2 N_{max} for every step in J. It is possible to push N_{A3max} and these channel truncations even higher and may be needed in the future for increased accuracy.

Table III gives a summary of the levels of convergence achieved in the present calculations. These are unextrapolated

results from complete model spaces for the purposes of comparison to existing and future results and experiment. Extrapolated results for ^{6}Li will be given below. We strongly advise the reader that the specific choice of λ is less important than the λ *dependence* in the final results. The λ dependence is the indicator that many-body forces are being induced to account for the renormalized components. Here we choose to display λ's $= 1.0$ and 1.8 fm^{-1} as they reach over the range of λ dependence in this work. For the potentials AV18 and CD-Bonn the value for $NN + NNN$-induced in the table corresponds to the unevolved minimum. The optimal frequency for the unevolved potential in these cases is $\hbar\Omega \simeq 52$ MeV and these values are quoted in the table.

IV. EVOLUTION OF MANY-BODY FORCES

In Fig. 8, the general flow of an SRG evolved nuclear Hamiltonian is illustrated. The ground-state energy of the triton is plotted as a function of the flow parameter λ from ∞, which is the initial (or "bare") interaction, toward $\lambda = 0$. We used $N_{A2max} = 196$, $N_{A3max} = 36$, and $\hbar\Omega = 20$ MeV, for

TABLE III. Results for binding energy in all calculations for ^{3}H and ^{4}He. All errors for SRG results are convergence margins at the quoted basis size. The columns marked *NN+3N* show $NN + NNN$-induced values except for rows that include an initial *NNN*. Basis sizes are $N_{A3max} = 40$ and $N_{A2max} = 196$ for all except N^{3}LO calculations used $N_{A3max} = 32$.

Nucleus/ potential	$\hbar\Omega$	*NN*-only $\lambda = 1.0$	*NN* + 3*N* $\lambda = 1.0$	*NN*-only $\lambda = 1.8$	*NN* + 3*N* $\lambda = 1.8$	LS
^{3}H, AV18	28/52	−7.487(1)	−7.486(40)	−8.467(1)	−7.486(40)	−7.62(0)
CD-Bonn	28/52	−7.505(1)	−7.863(40)	−8.553(1)	−7.863(40)	−7.99(1)
N^{3}LO	20	−7.471(2)	−7.852(5)	−8.351(1)	−7.852(5)	−7.852(5)
+*NNN*	20	−	−8.473(5)	−	−8.473(5)	−8.473(5)
^{4}He, AV18	44	−24.419(23)	−24.339(14)	−29.267(15)	−23.904(25)	−24.23(1)
CD-Bonn	44	−24.484(16)	−26.217(9)	−29.739(11)	−25.926(17)	−26.1(1)
N^{3}LO	28	−24.284(0)	−25.641(1)	−28.446(1)	−25.325(1)	−25.39(1)
+*NNN*	28	−	−28.661(3)	−	−28.464(2)	−28.50(2)

which all energies are converged to better than 10 keV. The previous work [3] used a less stringent $N_{A2max} = N_{A3max} = 36$. However, those results are within 1 keV of the current calculations, showing that the larger N_{A2max} is not critical for ^{3}H.

We first consider the *NN*-only curve (squares). If H_λ is evolved in only an $A = 2$ system, higher-body induced pieces are not included. The resulting energy calculations will be only approximately unitary for $A > 2$ and the ground-state energy will vary with λ (squares). Keeping the induced *NNN* matrix elements, by performing the $A = 3$ evolution, yields a flat line (circles), which confirms an exactly unitary transformation in that sector. The line is equally flat if an initial *NNN* is included (diamonds). Note that the net induced three-body is comparable to the initial *NNN* contribution and thus is of natural size.

The shape of the *NN*-only curve, first increasing binding and then rebounding, can be understood from the fact that early in the evolution the high-momentum matrix elements are most affected by the 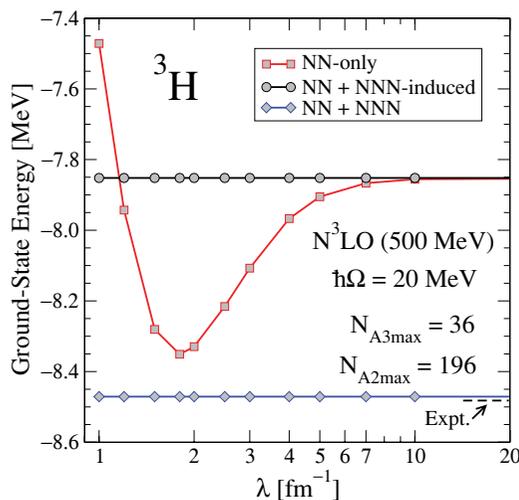transformations. These are predominantly the short-range repulsive parts of the potential and are transformed into strength in the induced *NNN* matrix elements. As the evolution progresses to lower-momentum scales the more attractive parts of the potential are affected, causing a rebound in the *NN*-only result. Note that all this information is not lost but merely reorganized into *NNN* terms, and when we keep those terms we regain the unitary result. This analysis is supported by studies in one-dimensional models that showed purely attractive initial potentials to have monotonically decreasing binding energy [13,21].

In Fig. 9, we examine the SRG evolution in λ for ^{4}He using a chiral N^{3}LO potential [29] with $\hbar\Omega = 36$ and 28 MeV, the dashed and solid sets respectively. The $\langle V_\lambda^{(2)} \rangle$ and $\langle V_\lambda^{(3)} \rangle$ matrix elements were evolved with basis sizes $N_{A2max} = 196$ and $N_{A3max} = 32$ and then truncated to $N_{max} = 18$ at each

FIG. 8. (Color online) Ground-state energy of ^{3}H as a function of the SRG evolution parameter, λ. See Table I for the nomenclature of the curves. The calculations use $N_{A2max} = 196$, $N_{A3max} = 36$, and $\hbar\Omega = 20$ MeV.
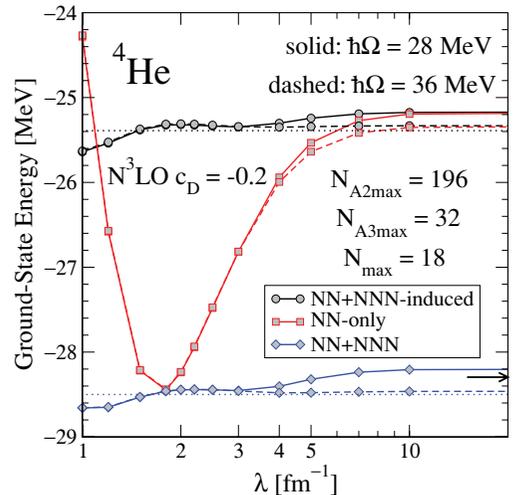

FIG. 9. (Color online) Ground-state energy of ^{4}He as a function of the SRG evolution parameter, λ. Note the comparison of two values for $\hbar\Omega$ (solid and dashed) and the best LS results (dotted). Here, $N_{A2max} = 196$ and $N_{A3max} = 32$ compared to $N_{A2max} = N_{A3max} = 28$ for the prior work [3]. The results here are converged to within 10 keV of those from Ref. [3]. See Table I for the nomenclature of the curves. Note the comparison of two values for $\hbar\Omega$ (solid and dashed) and the best LS results (dotted). The thick arrow indicates the experimental value.
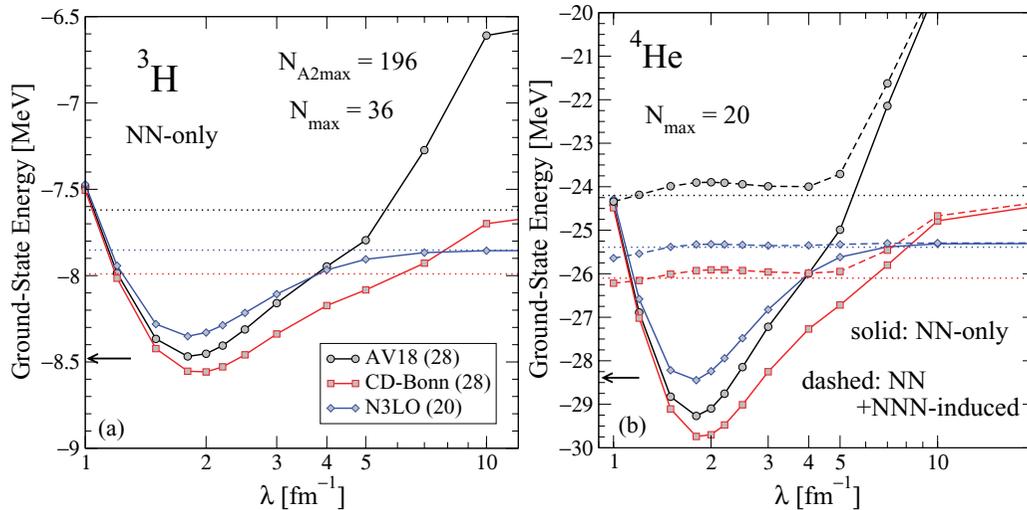
FIG. 10. (Color online) Ground-state energy of (a) ^{3}H and (b) ^{4}He as a function of λ, starting from Hamiltonians based on CD-Bonn [28], Argonne V_{18} [27], and N^{3}LO [29]. See Table I for the nomenclature of the curves. Here we used $\hbar\Omega = 28/28/20$ and $44/44/28$ for ^{3}H and ^{4}He, respectively. The dotted lines show the converged LS results for each potential. For ^{3}H these values are AV18 $= -7.62$, CD-Bonn $= -7.99$, and N^{3}LO $= -7.85$.

λ to diagonalize ^{4}He. Again, the higher N_{A2max} has little impact on the final results for this nucleus. The *NN*-only curve has the characteristic shape discussed above. When the induced *NNN* is included, the λ dependence is significantly reduced. The pattern depends only slightly on the inclusion of the initial *NNN* interaction. In both cases the dotted line represents the converged value for the initial Hamiltonian using a Lee-Suzuki–based procedure. The residual λ dependence is due to missing induced four-body forces.

At large λ, the discrepancy with the dotted line is due to a lack of convergence for unevolved potentials at $N_{max} = 18$, but at $\lambda < 3$ fm^{-1} SRG decoupling takes over and the discrepancy is due to short-range induced four-body forces. This transition is emphasized by showing the calculation at two different values of $\hbar\Omega$. The point in λ where they meet is an indicator of the momentum scale at which the evolving Hamiltonian is converged with $N_{max} = 18$. All the information included in the initial Hamiltonian at N_{A3max} has been transformed into the smaller basis defined by N_{max}. Any residual difference between values of $\hbar\Omega$ (invisible on this scale) indicate the level of convergence with respect to the included $\langle V_\lambda^{(3)} \rangle$ matrix elements defined by N_{A3max}.

In the three-body-inclusive curves the discrepancy due to induced four-body forces is about 50 keV net at $\lambda = 2$ fm^{-1}. This is small compared to the rough estimate in Ref. [33] that the contribution from the long-ranged part of the N^{3}LO four-nucleon force to ^{4}He binding is of order a few hundred keV. If needed, we could evolve four-body matrix elements in $A = 4$ and will do so when nuclear structure codes can accommodate them.

Figure 10 compares the flow of ^{3}H and ^{4}He binding energies for several initial Hamiltonians, AV18 [27], CD-Bonn [28], and N^{3}LO [29]. For ^{3}H we have used harmonic oscillator frequencies $\hbar\Omega = 28$, 28, and 20 MeV, respectively. For ^{4}He these optimal frequencies are $\hbar\Omega = 44$, 44, and 28 MeV, respectively. The general shape of all the *NN*-only curves is

quite similar here with a initial dip in binding and then a turn over at $\lambda = 1.8$ fm^{-1}. Evolution to low λ (< 2.0 fm^{-1}) of different initial Hamiltonians at $A = 2$ produce a very similar evolved form [18]. Previously this had only been observed at the level of comparing selected two-body matrix elements. Here we show that observables at $A > 2$ also exhibit this behavior. The *NN*-only points for all three initial Hamiltonians converge as λ decreases past 1.8. Note that the values for the unevolved potentials AV18 and CD-Bonn do not approach the Lee-Suzuki results because these potentials require a larger UV cutoff and therefore a larger $\hbar\Omega$ ($\simeq 52$) or N_{max} for convergence. The converged values for the bare potentials are quoted in Table III and would be the equivalent of the unitary line shown in Fig. 8.

Of course, we should not expect the $NN + NNN$-induced calculations to produce identical results at small λ because they are not equivalent Hamiltonians at the $A = 3$ level. However, their very similar shape indicates a specific scale dependence of three- and four-body forces generated during evolution. This is reminiscent of evolution of the chiral interaction in Fig. 9 with and without initial *NNN*, where the shape is similar but shifted by the initial difference. This is a promising indication of a universality phenomenon. A full test of this idea will require coding analogous three-body interactions for the other initial potentials (i.e., IL-IX for AV18) and evolving other initial *NN* interactions.

Figure 11 shows extrapolated ground-state energies for ^{6}Li at different values of λ. We used truncations $N_{A2max} = 300$ and $N_{A3max} = 40$ and performed the final diagonalization to $N_{max} = 8$. The gray bands represent the best Lee-Suzuki results available for *NN*-only and $NN + NNN$ initial interactions, with error estimates. The analogous truncations for these calculations were $N_{A2max} = 400$ and $N_{A3max} = 40$ with ^{6}Li being calculated up to $N_{max} = 14$ for *NN*-only. The results are 28.5 ± 0.5 MeV without and 32.5 ± 0.5 MeV with initial three-body forces.
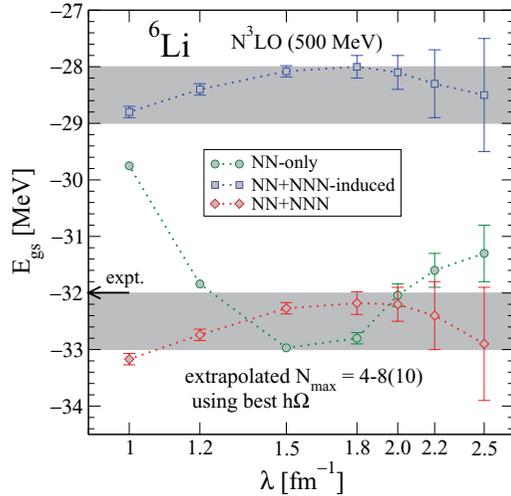
FIG. 11. (Color online) Extrapolated ground-state energy of ^{6}Li as a function of the SRG evolution parameter, λ. Error bars are based on variation of the minimum in $\hbar\Omega$ as discussed in the text. The truncations used were $N_{A2max} = 300$ and $N_{A3max} = 40$.

The λ dependence is shown for the lower values where the result is near convergence. The results plotted here are obtained from the extrapolation procedure previously described. This procedure accounts for the variation, with λ, of the minimum $\hbar\Omega$ and extrapolates in N_{max} the converged binding energy. The error bars are dependent on the range in $\hbar\Omega$ for which we have results. For any given λ the error bars will be larger if the optimal $\hbar\Omega$ is not present in the data set used for extrapolation. In fact, the extrapolation tends to predict too low (more negative) as measured by the predictions of $N_{max} = 10$ points in the *NN*-only curve. This feature has also been confirmed as we systematically added to the data set for the λ's with the largest error bars; the extrapolated points rose with better values of $\hbar\Omega$, flattening the curve and reducing the apparent λ dependence.

The hierarchy of induced many-body forces can be assessed in Fig. 11 by comparing the spread in the *NN*-only curve to that of the *NN* + *NNN* curves. To do so, note that the *NN*-only curve must coincide with the LS result at $\lambda = \infty$. The spread in λ has been reduced from 4 to <1 MeV. The majority of induced many-body forces missing from the *NN*-only curve is due to three-body forces subsequently included in the other curves. Note that the shape of the evolution curve is very similar to those of ^{4}He from any of the initial potentials used—a gentle rise to 1.8 and a slightly steeper slope down through 1.0. We interpret this to indicate that the majority of many-body ($A \geqslant 4$) forces induced are for $A = 4$ and that five- and six-body forces are significantly smaller. This is consistent with the expected hierarchical flow of induced many-body forces [13]. The spread here is roughly 1 MeV, compared to the 30–60 keV found in ^{4}He calculations.

Our *NN*-only curve is almost identical in shape to previous momentum space studies, despite the difference in initial Hamiltonians used. The previous study used only the neutron-proton interaction for all *NN* interactions while we have used the full isospin-breaking potential. The results

are systematically shifted up (in the previous study ^{6}Li was overbound by $\simeq 1$ MeV) in relation to the *NNN*-inclusive curves. The error bars for the same N_{max} are roughly the same as the previous work, confirming that *NN*-only calculations are good predictors of appropriate $\hbar\Omega$ values.

Note that the many-body forces do not explode as previously feared and that evolution to lower λ may not be unreasonable. While previous *NN*-only studies showed induced three-nucleon forces growing uncontrolled below $\lambda = 1.5$, we see that inclusion of these matrix elements produces a more gentle λ dependence. So evolving to lower λ to improve convergence may be useful in future calculations. Recent results [25] suggest that, for the choice of SRG generator in Eq. (2), the many-body forces may grow with A, so monitoring in the rest of the p shell (with adequate codes) is vital. Alternative choices for the SRG generator and sophisticated extrapolation techniques may play a central role.

V. HIERARCHY

In order to more fully understand the SRG evolution we can trace the individual parts of the Hamiltonian. Figure 12 shows the ^{3}H and ^{4}He ground-state expectation values of individual components of the evolving Hamiltonian as a function of λ. The insets show an increased scale for closer inspection of three- and four-body expectation values. Here a hierarchy of induced many-body forces is evident. The magnitude of variation in λ for each curve differs by approximately an order of magnitude. Cancellations between T_{rel} and V_{NN} are reduced significantly over the course of the evolution. The strength of matrix elements at large momenta is being reorganized into (shifted to) lower-momentum matrix elements. Hence the absolute values of the expectation values $\langle T_{rel} \rangle$ and $\langle V_{NN} \rangle$ are reduced.

Also, note the correspondence between the $\langle V_{3N} \rangle$ curve and *NN*-only evolution curves such as in Figs. 8 and 9. The size of the three-body force reaches a minimum corresponding to the point ($\lambda \simeq 1.8$ fm^{-1}) of maximum binding achieved by the *NN*-only calculations. This is simply the explicit plotting of the many-body forces that is implied by the approximately unitary curves shown in Sec. IV. In this case, the induced three-body forces effectively cancel out the initial three-body terms; the expectation value, $\langle V_{3N} \rangle$, drops almost to zero (Table IV).

To make a connection between the individual terms in the three-body interaction evolution and the running of the ground-state energy, we need the evolution equations for the *expectation value* of $V_s^{(3)}$ in the ground state. Denoting the ground-state wave function for the A-particle system by $|\psi_s^A\rangle$, it evolves according to (it is convenient here to use the flow parameter $s = 1/\lambda^4$)

$$\left|\psi_s^A\right\rangle = U_s\left|\psi_{s=0}^A\right\rangle, \qquad \frac{d}{ds}\left|\psi_s^A\right\rangle = \eta_s\left|\psi_s^A\right\rangle, \qquad (9)$$

where U_s is the SRG unitary transformation at s and

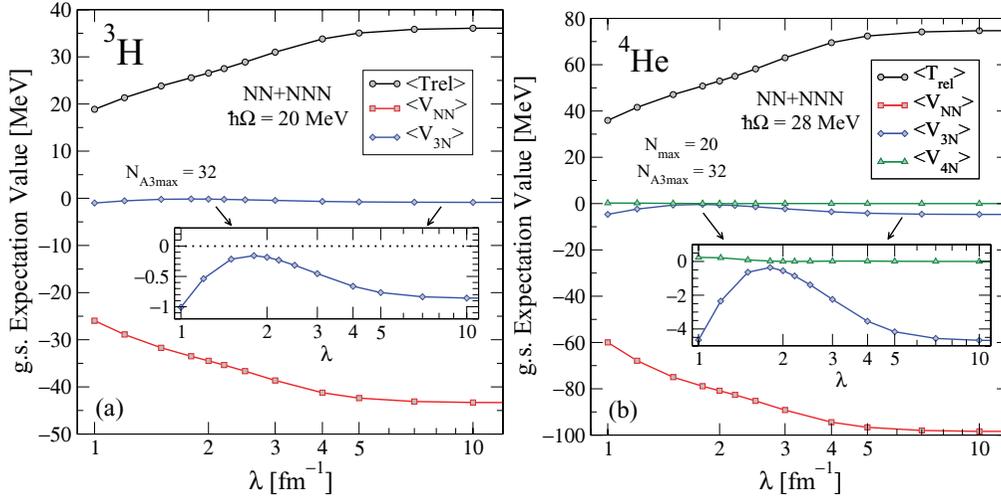$$\eta_s = \frac{dU_s}{ds}U_s^\dagger = -\eta_s^\dagger. \qquad (10)$$

FIG. 12. (Color online) Expectation value of the components of the nuclear interaction in the (a) ^{3}H and (b) ^{4}He ground states as a function of the SRG parameter λ. The initial interaction was N^{3}LO NN [29] and N^{2}LO NNN at $\hbar\Omega = 20$ and 28 MeV (left and right) and $N_{A3max} = 32$ with the ^{4}He final truncation at $N_{max} = 18$. The insets show expanded details for the three- and four-body forces.

Then the matrix element of an operator O_s evolves according to

$$\frac{d}{ds}\langle\psi_s^A|O_s|\psi_s^A\rangle = \langle\psi_s^A|\frac{dO_s}{ds} - [\eta_s, O_s]|\psi_s^A\rangle. \quad (11)$$

If the operator O_s is transformed as $O_s = U_s O_{s=0} U_s^\dagger$, then the matrix element on the right-hand side of Eq. ((11)) vanishes, as when $O_s = H_s$.

However, if we wish to see how one part of H_s evolves, such as the expectation value of $V^{(3)}$, we obtain

$$\frac{d}{ds}\langle\psi_s^A|V_s^{(3)}|\psi_s^A\rangle = \langle\psi_s^A|\frac{dV_s^{(3)}}{ds} - [\eta_s, V_s^{(3)}]|\psi_s^A\rangle, \quad (12)$$

which does not give zero in general because $V_s^{(3)} \neq U_s V_{s=0}^{(3)} U_s^\dagger$. In the two-particle case, the analog of Eq. (12) gives $d\langle V^{(2)}\rangle/ds = \langle[\eta_s, T_{rel}]\rangle$. In the three-particle case, we can

TABLE IV. Results for extrapolated binding energy of ^{6}Li at various values of λ and including error bars from the extrapolation. The analogous results from Lee-Suzuki calculations are -28.5 ± 0.5 MeV for NN-only and $NN + NNN$-induced and -32.5 ± 0.5 MeV for $NN + NNN$. The experimental value is -31.99 MeV. The $\hbar\Omega$ and range in N_{max} used for each extrapolation is also quoted.

λ	Best $\hbar\Omega$	NN-only (N_{max} 4–10)	$NN + NNN$-induced (N_{max} 4–8)	$NN + NNN$ (N_{max} 4–8)
2.5	24	-31.3 ± 0.5	-28.5 ± 1.0	-32.9 ± 1.0
2.2	20[a]	-31.6 ± 0.3	-28.3 ± 0.6	-32.4 ± 0.6
2.0	20	-32.0 ± 0.2	-28.1 ± 0.3	-32.2 ± 0.3
1.8	16	-32.8 ± 0.1	-28.0 ± 0.2	-32.2 ± 0.2
1.5	16	-33.00 ± 0.05	-28.1 ± 0.1	-32.3 ± 0.1
1.2	16	-31.85 ± 0.05	-28.4 ± 0.1	-32.75 ± 0.1
1.0	16	-29.75 ± 0.02	-28.8 ± 0.1	-33.2 ± 0.1

[a]This one point has a different optimal $\hbar\Omega$ for NN-only at $\hbar\Omega = 24$.

expand Eq. (12) as

$$\frac{d}{ds}\langle\psi_s^A|V_s^{(3)}|\psi_s^A\rangle$$
$$= \langle\psi_s^A|[\eta_s, H_s]_3 - [\eta_s, V_s^{(3)}]|\psi_s^A\rangle$$
$$= \langle\psi_s^A|[\overline{V}_s^{(3)}, T_{rel}] + [\overline{V}_s^{(2)}, V_s^{(2)}]_c + [\overline{V}_s^{(2)}, V_s^{(3)}]$$
$$+ [\overline{V}_s^{(3)}, V_s^{(2)}] + [\overline{V}_s^{(3)}, V_s^{(3)}] - [\overline{V}_s^{(2)}, V_s^{(3)}]$$
$$- [\overline{V}_s^{(3)}, V_s^{(3)}]|\psi_s^A\rangle$$
$$= \langle\psi_s^A|[\overline{V}_s^{(3)}, H_s] + [\overline{V}_s^{(2)}, V_s^{(2)}]_c - [\overline{V}_s^{(3)}, V_s^{(3)}]|\psi_s^A\rangle$$
$$= \langle\psi_s^A|[\overline{V}_s^{(2)}, V_s^{(2)}]_c - [\overline{V}_s^{(3)}, V_s^{(3)}]|\psi_s^A\rangle, \quad (13)$$

where $\overline{V}_s^{(2)}$ and $\overline{V}_s^{(3)}$ are the commutators $\overline{V}_s^{(2)} \equiv [T_{rel}, V_s^{(2)}]$ and $\overline{V}_s^{(3)} \equiv [T_{rel}, V_s^{(3)}]$. In the third line, the expectation value of the commutator, $[\overline{V}_s^{(3)}, H_s]$, vanishes identically.

The subscript "c" in the first term indicates that only connected parts of this commutator have been kept and refers to a diagrammatic formalism developed in Ref. [19]. Computing $[\overline{V}_s^{(2)}, V^{(2)}]$ in the three-particle space involves all nucleons democratically. However, commutators which leave one nucleon as a spectator cancel out in the $A = 2$ sector. So, we must compute $[\overline{V}_s^{(2)}, V^{(2)}]$ for the $A = 2$ sector and embed it in $A = 3$ so we can isolate the piece that affects the evolution of $V^{(3)}$. In general, this subtraction is required at all sectors in A, and the "c" here indicates that this procedure has been done.

In Fig. 13 we show the ground-state expectation values of the terms in Eq. (13) for the triton. The left panel shows the calculations with just-induced NNN interactions and the right panel with an initial three-body force. It is most useful for our analysis to convert from derivatives with respect to s to derivatives with respect to λ using $\frac{d}{ds} = -\frac{\lambda^5}{4}\frac{d}{d\lambda}$. The dominant contribution to the evolution of the three-body potential matrix
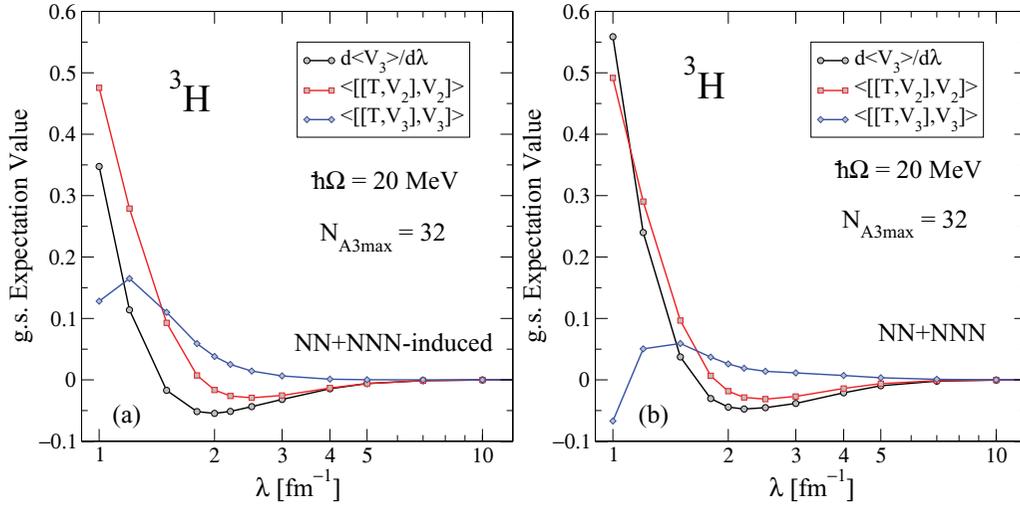
FIG. 13. (Color online) Contributions from individual terms to $d\langle V_\lambda^{(3)}\rangle/d\lambda$; the flow of the triton ground-state expectation value of the three-body potential. The calculation is done (a) without and (b) with an initial three-body interaction.

element is the two-body connected part, $[\overline{V}_s^{(2)}, V_s^{(2)}]_c$. This dominance is stronger here than seen in a one-dimensional analog [13], perhaps due to a stronger initial hierarchy in the EFT compared to the initial conditions chosen in one dimension. Again, the evolution of three-body matrix elements depends on the interplay between long- and short-range, attractive and repulsive, parts, which lead to scale-dependent inflection points and slopes.

We can repeat the above analysis for $A = 4$ and obtain

$$\frac{d}{ds}\langle\psi_s^{(4)}|V_s^{(4)}|\psi_s^{(4)}\rangle = \langle\psi_s^{(4)}|\left[\overline{V}_s^{(2)}, V_s^{(3)}\right]_c + \left[\overline{V}_s^{(3)}, V_s^{(2)}\right]_c$$
$$+ \left[\overline{V}_s^{(3)}, V_s^{(3)}\right]_c - \left[\overline{V}_s^{(4)}, V_s^{(4)}\right]|\psi_s^{(4)}\rangle,$$

$$(14)$$

where we find no fully connected terms with only two-body forces. Again, disconnected terms involving two- and

three-body potentials cancel out in the lower sectors. The leading terms are commutators with one $V_s^{(2)}$ and one $V_s^{(3)}$, followed by connected terms quadratic in $V_s^{(3)}$ and one term quadratic in $V_s^{(4)}$. All terms are small and additional cancellations among them may further suppress the four-body contribution. Thus, the initial hierarchy of many-body forces suggests that induced four-body (and higher-body) forces will be small.

In Fig. 14 we plot these contributions to the evolution of the four-body expectation value. The left panel shows the calculations with just-induced *NNN* interactions and the right panel includes initial three-body forces. Again, it is more useful to convert the derivatives in s to derivatives in λ. The interplay of contributions is much more complicated than for $A = 3$. We can see cancellations between one commutator involving $V_s^{(2)}$ and $V_s^{(3)}$ (blue diamonds) and the term quadratic in $V_s^{(3)}$ (green triangles). This is in slight contrast to the analogous case in one dimension where all
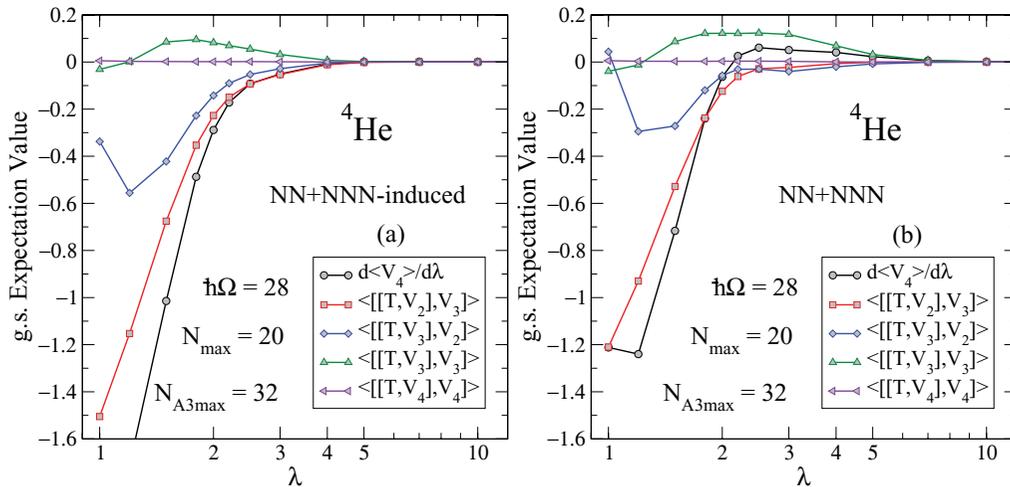

FIG. 14. (Color online) Contributions of the terms in Eq. (14) to $d\langle V_\lambda^{(4)}\rangle/d\lambda$, the evolving ^{4}He ground-state expectation value of the four-body force. The calculation is done (a) without and (b) with an initial three-body interaction.

four terms were involved in less straightforward cancellations. No terms quadratic in $V_s^{(2)}$ appear because no connected diagrams can be constructed for the four-particle evolution. The total derivative of $V_s^{(4)}$ is small until below $\lambda = 2$. Again the dominant contribution to the flow is the lowest-order commutator, and no feedback in $V_s^{(4)}$ is present.

There is room here for dependence of the induced many-body forces on the strength of the initial three-body potential and Fig. 14 supports this as far as $A = 4$. Forthcoming results [25] provide evidence of such dependence increasing with A. Other forms of SRG, such as one with the replacement $T_{\rm rel} \rightarrow T_{\rm rel} + V_{2\pi}$, may be useful in controlling the renormalization of the long-range parts of the initial potential.

We also note that any complete analysis of the growth of induced many-body forces must involve converged or extrapolated results at the optimal $\hbar\Omega$ for each λ. The analysis tool shown here is only meaningful when viewed at a single $\hbar\Omega$ over the course of evolution in λ and direct comparison to plots of the type shown in Fig. 14 is difficult.

VI. OBSERVABLES

While accurate reproduction of nuclear binding energies is the first step in nuclear structure calculations, other observables can offer additional information about the effects of renormalizing high-energy degrees of freedom, short-range correlations, and other details of a properly fit initial Hamiltonian. While we know that the harmonic oscillator basis is not an ideal environment for certain long-ranged observables, such

as the rms radius, we have existing Lee-Suzuki renormalized benchmarks with which to compare. And electromagnetic transitions, such as $B(E2)$'s and $B(M1)$'s, are notoriously difficult both to calculate and to measure, making this an important area of prediction for theory. All such observables are an important next test in understanding the quality of the many-body wave functions resulting from SRG-evolved interactions. Here we present a small sampling of results, focusing on convergence patterns.

Here we are plotting the unevolved operator expectation value in the evolved wave function. This is a reasonable way to visualize the effect of evolution on the structure with respect to particular operator. However, consistent renormalization of the operators themselves is an important part of a robust nuclear structure program. Work along these lines is proceeding and is partly presented in Ref. [14]. Extending beyond $A = 2$ will be covered in a forthcoming article.

Shown in Figs. 15(a)–15(e) are selected observables for ^{6}Li as a function of $N_{\rm max}$ up to $N_{\rm max} = 8$. Included are simple extrapolation curves shown by the dotted lines extending from the data points. Table V shows the values for $N_{\rm max} = 8$ at select values of λ. In all cases the extrapolated values compare well to the established Lee-Suzuki–based results but show room for improvement with respect to the experimental values. Note the small scales on some of the plots, especially the quadrupole moment and $B(M1;2^+1 \rightarrow 1^+0)$.

Some of these observables exhibit a nonvariational pattern in $N_{\rm max}$, such as the quadrupole moment and the $B(M1)$ shown here. These operators have strong coupling between shells of $N_{\rm max}$ and $N_{\rm max} + 2$ that result in complex cancellations from
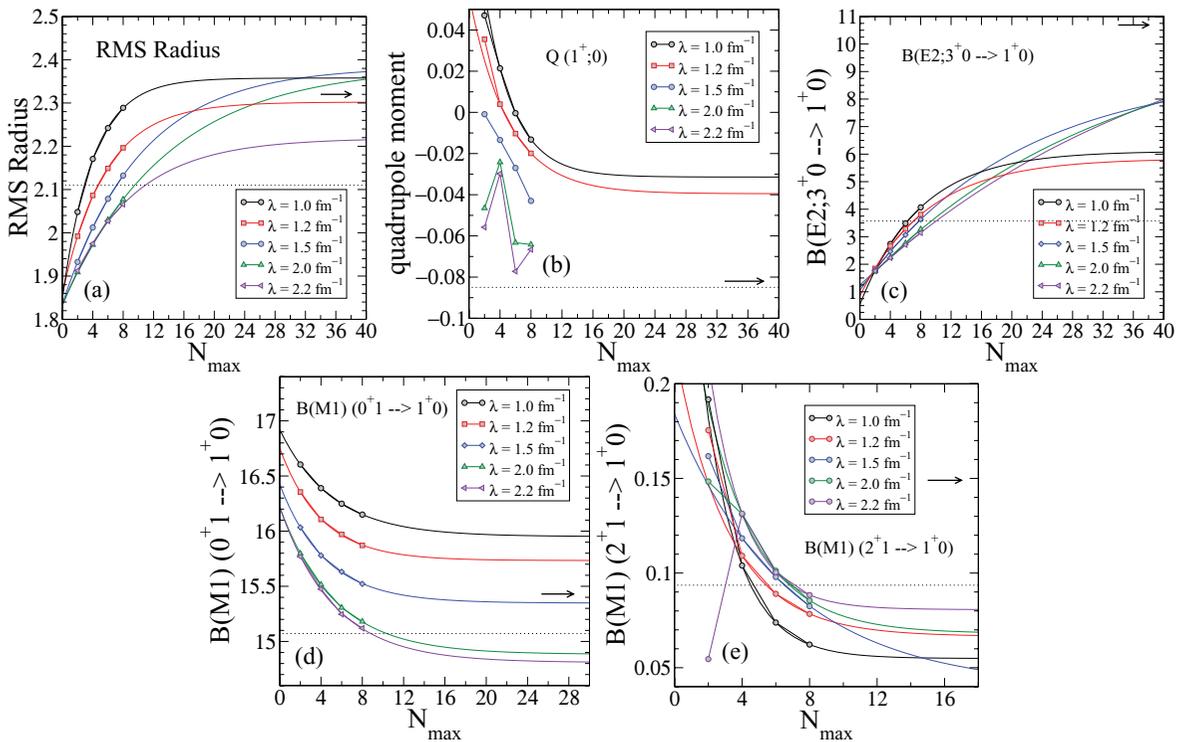

FIG. 15. (Color online) Various observables (a)–(e) in ^{6}Li as a function of $N_{\rm max}$ for select λ's. These results are with included initial *NNN* forces and $N_{\rm A2max} = 300$ and $N_{\rm A3max} = 40$ and $\hbar\Omega = 20$ MeV. The arrow shows the experimental value and the dotted line shows the best LS result.

TABLE V. Results for selected properties of ^{6}Li. Here we choose $\lambda = 1.0$ and 1.2 fm^{-1} due to their convergence properties. These results were obtained in a basis space with $N_{\max} = 8$ and $\hbar\Omega = 20$. All results have included initial $3N$ forces at N^{2}LO. The LS results were obtained at $N_{\max} = 8$ with $\hbar\Omega = 13$ MeV [36]. Note that $\hbar\Omega$ values for LS and SRG procedures do not necessarily correspond to one another.

Observable	$\lambda = 1.0$	$\lambda = 1.2$	Expt.	LS
r_p (fm)	2.2841	2.1913	2.32(3)	2.110
$Q(1_1^+0)$ (e fm^2)	-0.0132	-0.0199	$-0.082(2)$	-0.085
$B(E2; 3_1^+0 \to 1_1^+0)$	4.0663	3.8087	10.69(84)	3.5725
$B(M1; 0_1^+1 \to 1_1^+0)$	16.1499	15.8706	15.43(32)	15.0717
$B(M1; 2_1^+1 \to 1_1^+0)$	0.0622	0.0784	0.149(27)	0.0936

one truncation to another. However, SRG evolution seems to improve the variational properties of these observables. Access to larger $N_{\max}$ model spaces will facilitate further study of these quantities.

VII. CONCLUSIONS

We have presented *ab initio* calculations of several light nuclei using SRG-evolved three-nucleon forces. The results have smooth convergence qualities with respect to basis size, which enable reliable extrapolations. The extrapolated (and converged where available) values are within the error bars of the best existing Lee-Suzuki–based calculations. Investigating the λ dependence of induced many-body forces, we find that they do not grow substantially as λ is lowered and the range of these effects is within the established LS error bars. Analyzing the mechanism of flow for many-body terms reveals that the SRG is driven by the natural hierarchy of the initial Hamiltonian and that it preserves this hierarchy during evolution. This is qualitatively consistent with studies of the same in one dimension. Finally, we present some first results of various observables using SRG evolved many-body wave functions.

Our results here have focused mainly on ^{6}Li observables and analysis in the $A = 3$ and 4 sectors. However, the input Hamiltonian files produced for this work are universally valid for further calculations in the p-shell nuclei. Here, we were limited in basis size (to $N_{\max} = 8$ in ^{6}Li) but plan to apply the evolved potentials at larger A using codes capable of larger basis sizes. We are first interested in studies of ^{8}Be, ^{10}B, and ^{12}C, but this list will undoubtedly expand. Also, we hope these potentials will be applied using coupled-cluster methods for even larger A [38] and look forward to applications of SRG evolution to external operators. Our work here provides no indications of problems as high as ^{6}Li with T_{rel} as the SRG generator. Other forms of the SRG generator may be useful in controlling the growth of many-body forces in other nuclei.

In addition to the above ongoing work, we will apply the evolved three-body interactions developed here to NCSM/RGM calculations [39] of light nuclear reactions. The *NN*-only evolved interactions have so far produced good scattering and reaction results for *s*- and light *p*-shell nuclei. Adding the evolved three-body interaction to the NCSM/RGM formalism will further improve accuracy and allow us to extend its applicability to heavier *p*-shell and light *sd*-shell nuclei.

[1] S. K. Bogner, R. J. Furnstahl, S. Ramanan, and A. Schwenk, Nucl. Phys. A **784**, 79 (2007).

[2] S. K. Bogner *et al.*, Nucl. Phys. A **801**, 21 (2008).

[3] E. D. Jurgenson, P. Navrátil, and R. J. Furnstahl, Phys. Rev. Lett. **103**, 082501 (2009).

[4] S. D. Glazek and K. G. Wilson, Phys. Rev. D **48**, 5863 (1993); **49**, 4214 (1994).

[5] F. Wegner, Ann. de. Phys. **506**, 77 (1994); Phys. Rep. **348**, 77 (2001).

[6] J. Kehrein, *The Flow Equation Approach to Many-Particle Systems* (Springer, Berlin, 2006).

[7] S. K. Bogner, R. J. Furnstahl, and R. J. Perry, Phys. Rev. C **75**, 061001 (2007).

[8] S. K. Bogner, R. J. Furnstahl, R. J. Perry, and A. Schwenk, Phys. Lett. B **649**, 488 (2007).

[9] R. Roth, S. Reinhardt, and H. Hergert, Phys. Rev. C **77**, 064003 (2008).

[10] K. Suzuki and S. Y. Lee, Prog. Theor. Phys. **64**, 2091 (1980).

[11] P. Navrátil, J. P. Vary, and B. R. Barrett, Phys. Rev. Lett. **84**, 5728 (2000).

[12] E. Epelbaum, H. W. Hammer, and U. G. Meissner, Rev. Mod. Phys. **81**, 1773 (2009).

[13] E. D. Jurgenson and R. J. Furnstahl, Nucl. Phys. A **818**, 152 (2009).

[14] E. R. Anderson, S. K. Bogner, R. J. Furnstahl, and R. J. Perry, Phys. Rev. C **82**, 054001 (2010)

[15] E. D. Jurgenson, S. K. Bogner, R. J. Furnstahl, and R. J. Perry, Phys. Rev. C **78**, 014003 (2008).

[16] S. D. Glazek and R. J. Perry, Phys. Rev. D **78**, 045011 (2008).

[17] E. Anderson, S. K. Bogner, R. J. Furnstahl, E. D. Jurgenson, R. J. Perry, and A. Schwenk, Phys. Rev. C **77**, 037001 (2008).

[18] S. K. Bogner, R. J. Furnstahl, and A. Schwenk, Prog. Part. Nucl. Phys. **65**, 94 (2010).

[19] S. K. Bogner, R. J. Furnstahl, and R. J. Perry, Annals Phys. **323**, 1478 (2008).

[20] P. Navrátil, S. Quaglioni, I. Stetcu, and B. R. Barrett, J. Phys. G **36**, 083101 (2009).

[21] E. D. Jurgenson, Ph.D. thesis, The Ohio State University, 2009.

[22] J. P. Vary, The Many-Fermion Dynamics Shell-Model Code, Iowa State University, 1992 (unpublished); J. P. Vary and D. C. Zheng, The Many-Fermion Dynamics Shell-Model Code, Iowa State University, 1994 (unpublished).

[23] R. Roth and P. Navrátil, Phys. Rev. Lett. **99**, 092501 (2007).

[24] R. Roth, Phys. Rev. C **79**, 064324 (2009).

[25] R. Roth (private communication).

[26] P. Maris, J. P. Vary, and A. M. Shirokov, Phys. Rev. C **79**, 014308 (2009).

[27] R. B. Wiringa, V. G. J. Stoks, and R. Schiavilla, Phys. Rev. C **51**, 38 (1995).

[28] R. Machleidt, Phys. Rev. C **63**, 024001 (2001).

[29] D. R. Entem and R. Machleidt, Phys. Rev. C **68**, 041001(R) (2003).

[30] E. Epelbaum, A. Nogga, W. Glockle, H. Kamada, Ulf-G. Meissner, and H. Witala, Phys. Rev. C **66**, 064001 (2002).

[31] P. Navrátil, Few-Body Syst. **41**, 117 (2007).

[32] D. Gazit, S. Quaglioni, and P. Navrátil, Phys. Rev. Lett. **103**, 102502 (2009).

[33] D. Rozpedzik *et al.*, Acta Phys. Polon. B **37**, 2889 (2006).

[34] A. Kievsky *et al.*, J. Phys G **35**, 063101 (2008).

[35] P. Navrátil and E. Caurier, Phys. Rev. C **69**, 014311 (2004).

[36] P. Navrátil, V. G. Gueorguiev, J. P. Vary, W. E. Ormand, and A. Nogga, Phys. Rev. Lett. **99**, 042501 (2007).

[37] A. Nogga, P. Navrátil, B. R. Barrett, and J. P. Vary, Phys. Rev. C **73**, 064002 (2006).

[38] G. Hagen, D. J. Dean, M. Hjorth-Jensen, T. Papenbrock, and A. Schwenk, Phys. Rev. C **76**, 044305 (2007).

[39] S. Quaglioni and P. Navrátil, Phys. Rev. Lett. **101**, 092501 (2008); Phys. Rev. C **79**, 044606 (2009).